

# Weakening of the Multi-Point Constraints in Modal Substructuring using Singular Value Decomposition

Miha Pogačar<sup>a</sup>, Gregor Čepon<sup>a,\*</sup>, Miha Boltežar<sup>a</sup>

<sup>a</sup> *University of Ljubljana, Faculty of Mechanical Engineering, Aškerčeva 6, 1000 Ljubljana, Slovenia*

## *Cite as:*

*Miha Pogačar, Gregor Čepon, Miha Boltežar, Weakening of the multi-point constraints in modal substructuring using singular value decomposition, Mechanical Systems and Signal Processing, 2022, <https://doi.org/10.1016/j.ymssp.2021.108109>*

---

## **Abstract**

Modal substructuring is an established subdomain of dynamic substructuring in which the handling of multi-point connections between subcomponents proves to be a problematic task. This is particularly the case with experimental models, where even small inconsistencies in the interface dynamics can greatly affect the accuracy of the substructuring process. An established solution to this problem is based on the projection of physical interface motion on the modal basis of one of the substructures. Although both the dimension and the origin of the projection basis prove to have a great impact on the accuracy of the substructuring prediction, the established procedures do not provide a general criterion for their appropriate selection. The aim of this paper is to propose an alternative weakening approach based on singular value decomposition (SVD) that enables the construction of a vector space and the establishment of a criterion for the selection of its dominant components. Considering two substructures involved in a certain step of a substructuring procedure, SVD is performed on the interface-related components of the substructures' concatenated modal bases. The dominant left singular vectors, therefore, embody the interface dynamics of both substructures and provide a consistent orthonormal basis for the

---

\*Corresponding author

*Email address:* [gregor.cepon@fs.uni-lj.si](mailto:gregor.cepon@fs.uni-lj.si) (Gregor Čepon)

constraint-weakening process. The proposed empiric criterion for estimating the required vector-space dimension is based on the magnitude of singular values. The efficiency of the proposed methodology is presented in comparison to the established modal-constraint approach with three numerical examples and an experimental-analytical transmission simulator coupling procedure. It is shown that the proposed singular vector constraint approach in conjunction with the criterion to estimate the weakening basis size, provides a consistent and reliable substructuring procedure.

*Keywords:* singular vector constraints, experimental-analytical substructuring, component mode synthesis, experimental modal analysis

---

## 1. Introduction

Dynamic substructuring (DS) is a well-established field in structural dynamics. DS methods are used to predict the dynamic response of a structure, obtained by a sequence of coupling and/or decoupling steps between the individual subcomponents with known dynamic properties. These properties can be characterized in several different ways, among which the three general approaches (spatial, spectral, and state) can be distinguished [1]. Several difficulties can arise when experimental models are introduced to the substructuring procedure [2], due to the inevitable experimental errors, limited testable frequency band, etc. Therefore, several recent studies explored different approaches to analyse [3, 4] and reduce [5–8] the impact of experimental errors.

Representation within the modal domain often proves to be a convenient form of a substructure’s spatial dynamic characterization, based on its modal parameters. Modal substructuring, also referred to as component-mode synthesis (CMS), is widely used in the realm of numerical simulations and provides quality substructuring predictions in real-world applications with a complex geometry [9] and pronounced damping [10]. In real-life applications, components are often bonded with multi-point or continuous connections, which are

particularly problematic for substructuring predictions, as some of the physical constraints are often redundant. Even in numerical simulations, only due to the discretization, this can lead to interface locking and consequently to an erroneous substructuring prediction. This issue is even more pronounced when experimental models are considered in the substructuring procedure due to the unavoidable measurement errors. This problem can be reduced by weakening the compatibility and equilibrium conditions, which is typically done using a suitable mode-shape-based projection basis [5].

Extensive research has been conducted in the field of experimental-analytical substructuring with multi-point connections. In [5, 11, 12] the concept of the transmission simulator method (TSM) was presented and a weak modal constraint formulation (modal constraints for fixture and subsystem - MCFS or simply modal constraints - MCs) was introduced. Later, the TSM was reformulated to enable direct implementation in finite-element software [13]. Furthermore, the phenomenon of negative mass and stiffness within the modal decoupling procedure was investigated in [14]. Within the TSM a truncated set of flexible fixture's mode shapes is used to satisfy the physical constraints in a least-squares sense. When applying modal constraints, both the selection of the modal basis as well as the number of contained mode shapes considered for the weakening process, can significantly affect the quality of the substructuring prediction. In addition, the modal basis embodies the global behavior and can therefore contain information that is unnecessary or redundant in terms of interface dynamics. A general guideline for determining the truncation limit is to select it in or near the frequency band of interest [5]; however, the appropriate selection seems to be very case-specific. As an alternative to the MCFS, singular vector constraints are briefly introduced in [1], based on the Singular Value Decomposition (SVD) of a coupled substructure-fixture modal response. Following this idea, an admittance-based singular vector constraint approach was proposed in our previous work [15].

In this paper a novel approach to singular vector constraints (SVCs) is presented, which can also be interpreted as an extension of the established modal

constraints. Instead of using the modal basis of a single substructure, the modal bases of two substructures are considered in the weakening process for each step in the substructuring procedure. Concatenated interface-related components of the modal bases are submitted to SVD. The resulting dominant left singular vectors represent an orthonormal vector space that embodies the interface motion of both substructures and seems to represent a consistent basis for the constraints-weakening process. Since the weakening basis is obtained using SVD, it is also possible to establish an empirical criterion based on the magnitude of singular values, to estimate the number of singular vectors required to describe the dominant interface motion. Note, that within the MC approach there is no general criterion available to select the optimal modal sub-basis for the constraints-weakening process. Compared to the established solutions, such an approach proves to have certain advantages. The generated weakening basis is richer and does not contain any redundant contributions, that might lead to interface locking. By an appropriate selection of the dominant vectors, the insignificant or noise-induced contributions are discarded.

The applicability of the proposed approach is demonstrated on three direct-coupling numerical examples, considering various system parameters. The singular vector constraint concept is also applied to the TSM and an experimental-numerical study is performed. The results demonstrate the efficiency of the proposed weakening procedure using singular vector constraints. Compared to the established modal-constraint approach, equivalent or better accuracy, as well as greater robustness, of the substructuring prediction can be achieved.

This paper is organized as follows. The next section summarizes the basic modal substructuring theory, followed by the presentation of weak constraint formulations and singular value decomposition. In Section 3 the proposed singular vector constraints methodology is outlined. In Section 4 the applicability of the proposed methodology is demonstrated and the TSM experimental-analytical study is presented in Section 5. Finally, conclusions are drawn in Section 6.

## 2. Theoretical background

### 2.1. Component mode synthesis - Primal formulation

In this section the basic theory of modal substructuring is presented, following the notation in [2]. For each substructure, the linear equations of motion in the physical domain can be written as<sup>1</sup>:

$$\mathbf{M}^{(s)} \ddot{\mathbf{u}}^{(s)} + \mathbf{C}^{(s)} \dot{\mathbf{u}}^{(s)} + \mathbf{K}^{(s)} \mathbf{u}^{(s)} = \mathbf{f}^{(s)} + \mathbf{g}^{(s)}, \quad (1)$$

where  $\mathbf{M}^{(s)}$ ,  $\mathbf{C}^{(s)}$  and  $\mathbf{K}^{(s)}$  are the mass, damping, and stiffness matrices of the substructure  $s$ . Vector  $\mathbf{u}$  denotes the substructure's degrees of freedom,  $\mathbf{f}^{(s)}$  is the external force vector, and  $\mathbf{g}^{(s)}$  is the vector of connecting forces with other substructures. Vectors  $\dot{\mathbf{u}}^{(s)}$  and  $\ddot{\mathbf{u}}^{(s)}$  denote the first and second time derivatives of the degrees of freedom, respectively. The equations of motion for a system of  $n$  substructures, for which the coupling or decoupling is to be performed, can be written in a block-diagonal form<sup>2</sup>:

$$\mathbf{M} \ddot{\mathbf{u}} + \mathbf{C} \dot{\mathbf{u}} + \mathbf{K} \mathbf{u} = \mathbf{f} + \mathbf{g}, \quad (2)$$

where:

$$\mathbf{M} = \text{diag} [\mathbf{M}^{(1)}, \dots, \mathbf{M}^{(n)}], \mathbf{C} = \text{diag} [\mathbf{C}^{(1)}, \dots, \mathbf{C}^{(n)}], \mathbf{K} = \text{diag} [\mathbf{K}^{(1)}, \dots, \mathbf{K}^{(n)}],$$

and  $\mathbf{u} = \{\mathbf{u}^{(1)}, \dots, \mathbf{u}^{(n)}\}^T$ ,  $\mathbf{f} = \{\mathbf{f}^{(1)}, \dots, \mathbf{f}^{(n)}\}^T$ ,  $\mathbf{g} = \{\mathbf{g}^{(1)}, \dots, \mathbf{g}^{(n)}\}^T$ .

The corresponding compatibility and equilibrium condition can be written as:

$$\mathbf{B} \mathbf{u} = \mathbf{0}, \quad (3)$$

$$\mathbf{L}^T \mathbf{g} = \mathbf{0}, \quad (4)$$

where the  $\mathbf{B}$  matrix operates on the interface degrees of freedom and the  $\mathbf{L}$  matrix is localizing the interface DoF in the global dual set of DoF. Assuming conforming discretizations of the interface,  $\mathbf{B}$  is a signed Boolean matrix and  $\mathbf{L}$

---

<sup>1</sup>For the sake of simplicity the explicit time dependency is omitted.

<sup>2</sup>Note, that if the decoupling of a substructure is required, the corresponding mass, damping and stiffness matrices in the global block-diagonal equation are to be assigned as negative.

is a Boolean matrix. The corresponding compatibility and equilibrium condition formulation is considered to be exact/strong. The system of Eqs. (2)–(4) describes the dynamic properties of the coupled/decoupled system of components. From this set of equations, the coupled system can be obtained in either the primal or dual formulation [2]. Within this paper, only the primal substructuring formulation in the modal domain is considered.

Modal substructuring or CMS refers to the methods where the substructures' dynamic properties are approximated in a reduction basis. The transformation of the physical DoF is performed by a reduction matrix  $\mathbf{R}$ , which typically contains some type of components' mode shapes:

$$\mathbf{u} \approx \mathbf{R} \boldsymbol{\eta}, \quad (5)$$

where  $\mathbf{R} = \text{diag} [\mathbf{R}^{(1)}, \dots, \mathbf{R}^{(n)}]$  and  $\boldsymbol{\eta}$  is a vector of generalized coordinates. The coupled/decoupled system of Eqs. (2)–(4) in the modal domain can be expressed as<sup>3</sup>:

$$\mathbf{M}_m \ddot{\boldsymbol{\eta}} + \mathbf{C}_m \dot{\boldsymbol{\eta}} + \mathbf{K}_m \boldsymbol{\eta} = \mathbf{f}_m + \mathbf{g}_m, \quad (6)$$

$$\mathbf{B}_m \boldsymbol{\eta} = \mathbf{0}, \quad (7)$$

$$\mathbf{L}_m^T \mathbf{g} = \mathbf{0}, \quad (8)$$

where:

$$\mathbf{M}_m = \mathbf{R}^T \mathbf{M} \mathbf{R}, \mathbf{C}_m = \mathbf{R}^T \mathbf{C} \mathbf{R}, \mathbf{K}_m = \mathbf{R}^T \mathbf{K} \mathbf{R}, \mathbf{f}_m = \mathbf{R}^T \mathbf{f}, \mathbf{g}_m = \mathbf{R}^T \mathbf{g},$$

and

$$\mathbf{B}_m = \mathbf{B} \mathbf{R}, \mathbf{L}_m = \text{null} [\mathbf{B}_m].$$

---

<sup>3</sup>When mass-normalized mode shapes are considered as a reduction basis, the following relations apply:  $\mathbf{M}_m = \text{diag} [\mathbf{I}^{(1)}, \dots, \mathbf{I}^{(n)}]$ ,  $\mathbf{C}_m = \text{diag} [2 \boldsymbol{\xi}_r^{(1)} \boldsymbol{\omega}_r^{(1)}, \dots, 2 \boldsymbol{\xi}_r^{(n)} \boldsymbol{\omega}_r^{(n)}]$ ,  $\mathbf{K}_m = \text{diag} [\boldsymbol{\omega}_r^{2(1)}, \dots, \boldsymbol{\omega}_r^{2(n)}]$ , where for a substructure  $s$ ,  $\mathbf{I}^{(s)}$  is an identity matrix, and  $\boldsymbol{\omega}_r^{2(s)}$  and  $\boldsymbol{\xi}_r^{(s)}$  are the diagonal matrices of the substructure's eigenvalues and the damping ratios, respectively.

Within the primal formulation, a unique set of generalized coordinates  $\boldsymbol{\xi}$  is used, following the relation:

$$\boldsymbol{\eta} = \mathbf{L}_m \boldsymbol{\xi}. \quad (9)$$

Note, that in order to enforce the interface assembly in a fully compatible way, matrix  $\mathbf{L}_m$  must span the null-space of  $\mathbf{B}_m$ . This weakens the equilibrium condition, as  $\mathbf{R}\mathbf{L}_m$  represents a subspace of  $\mathbf{L}$  [2]. By pre-multiplication with  $\mathbf{L}_m^T$ , the system of Eqs. (6)–(8) reduces to:

$$\tilde{\mathbf{M}}_m \ddot{\boldsymbol{\xi}} + \tilde{\mathbf{C}}_m \dot{\boldsymbol{\xi}} + \tilde{\mathbf{K}}_m \boldsymbol{\xi} = \tilde{\mathbf{f}}_m, \quad (10)$$

where:

$$\tilde{\mathbf{M}}_m = \mathbf{L}_m^T \mathbf{M}_m \mathbf{L}_m, \quad \tilde{\mathbf{C}}_m = \mathbf{L}_m^T \mathbf{C}_m \mathbf{L}_m, \quad \tilde{\mathbf{K}}_m = \mathbf{L}_m^T \mathbf{K}_m \mathbf{L}_m, \quad \text{and} \quad \tilde{\mathbf{f}}_m = \mathbf{L}_m^T \mathbf{f}_m.$$

## 2.2. Weak compatibility and equilibrium formulation

If the  $\mathbf{B}$  matrix is a signed Boolean matrix, the compatibility condition states that any pair of matching-interface degrees of freedom must have the same displacement<sup>4</sup>. Within the paper, the corresponding physical constraints are considered as exact/strong. When considering an interface with multiple connection points, an exact compatibility requirement might not be optimal for the substructuring procedure [5]. Moreover, the maximum number of constraints is limited by the sum of the substructures' modes<sup>5</sup>. Within the weak compatibility formulation, the number of constraints is reduced using a weakening matrix  $\mathbf{W}$ . Eqs. (7) and (8) can be rewritten as:

$$\mathbf{W} \mathbf{B}_m \boldsymbol{\eta} = \mathbf{0}, \quad (11)$$

$$\text{null} [\mathbf{W} \mathbf{B}_m]^T \mathbf{g} = \mathbf{0}. \quad (12)$$

---

<sup>4</sup>In general, non Boolean formulations of the  $\mathbf{B}$  operator can also be applied to link the non-conforming interface discretizations. Also, time-dependent formulations can be considered to track the sliding contacts [16].

<sup>5</sup>Considering the coupling of the substructures A and B with 20 modes each; the maximum number of applicable spatial point connections is limited to 13, resulting in a coupled AB structure with a single modal-DoF.

Within the established modal constraint approach, the modal basis of a selected substructure is used to formulate the weakening matrix. In the proposed methodology, singular vector constraints are considered as an alternative to form a suitable basis for the constraints-weakening procedure.

### 2.3. Singular Value Decomposition

Singular value decomposition of an arbitrary complex non-square matrix  $\mathbf{P}$  can be given as:

$$\mathbf{P} = \mathbf{U} \mathbf{S} \mathbf{V}^{\text{H}}, \quad (13)$$

where  $\mathbf{U}$  and  $\mathbf{V}$  are orthonormal matrices of the left and right singular vectors, respectively, and  $\mathbf{S}$  is a diagonal matrix of real, non-negative singular values, arranged in a descending order. The superscript  $[\ ]^{\text{H}}$  indicates a conjugate transpose.

When a set of concatenated mode shapes is considered as an input matrix, the left singular vectors can be considered as orthonormal response vectors and the right singular vectors reveal how each response vector participates in each of the input mode shapes. The corresponding singular values indicate the importance of each contribution[1].

## 3. Methodology

### 3.1. Proposed approach to singular vector constraints

To increase the clarity, the proposed novel methodology in this section is explained by considering the coupling procedure for substructures A and B, depicted in Figure 1. The modal parameters can be determined either numerically or experimentally [17, 18] for the selected DoF on the structures. In general, for a substructure  $s$ , the considered DoF can be divided into sets of internal DoF  $\mathbf{u}_i^{(s)}$  and boundary DoF  $\mathbf{u}_b^{(s)}$ , with the latter being located at the interface.

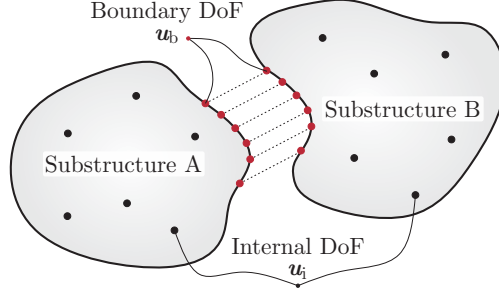


Figure 1: Coupling procedure of substructures A and B.

Within the paper a (truncated) set of  $N^{(s)}$  real mass-normalized free-interface mode shapes  $\Phi^{(s)}$  is considered as a reduction matrix. Following the distribution of DoFs, the mode-shape matrix can also be divided into boundary (index b) and internal (index i) components:

$$\Phi^{(s)} = \begin{Bmatrix} \Phi_b^{(s)} \\ \Phi_i^{(s)} \end{Bmatrix}. \quad (14)$$

The strong physical compatibility condition can be given as:

$$\mathbf{u}_b^{(A)} = \mathbf{u}_b^{(B)}. \quad (15)$$

A weak formulation of **modal constraints (MC)** is considered when the physical motion at the interface is projected onto the truncated modal basis of one of the substructures (A or B). In general, an arbitrary set of  $N_c$  mode shapes of substructure  $s$  can be used to generate a weakening matrix<sup>6</sup>:

$$\mathbf{W}_\Phi^{(s)} = \Phi_{b,N_c}^{(s)\dagger}, \quad (16)$$

where  $[\cdot]^\dagger$  denotes a generalized inverse. For example, consider using the modal basis of substructure A. In this case, a weak modal formulation of the compatibility condition (15) is given as:

$$\Phi_{b,N_c}^{(A)\dagger} \mathbf{u}_b^{(A)} = \Phi_{b,N_c}^{(A)\dagger} \mathbf{u}_b^{(B)}, \quad (17)$$

---

<sup>6</sup>Within the paper the first  $N_c$  mode shapes will be considered; however, in general an arbitrary combination can be used.

where the left-hand side of the equation is equal to the first  $N_c$  modal (generalized) coordinates  $\boldsymbol{\eta}_{N_c}^{(A)}$ . Therefore, physically, Eq. (17) constrains the modal coordinates of substructure A to their orthogonal projection onto the interface motion of substructure B [5]. Here, alternatively, the modal basis of substructure B could also be used. The origin of the selected projection basis and also the number of considered base vectors can significantly affect the resulting substructuring prediction. In general, it is difficult to select an appropriate projection basis (in terms of both the origin and the dimension). Therefore, this topic is addressed in our research in terms of proposing a SVD approach that enables the generation of a weakening basis together with a criterion to estimate the required number of constraints.

As an extension of the established modal weakening methodology, a new singular vector-based approach is proposed. The idea is to formulate a concatenated mode-shape matrix of substructures A and B (limited to the boundary DoF) and perform the singular value decomposition (SVD)<sup>7</sup>:

$$\mathbf{P} = \begin{bmatrix} \boldsymbol{\Phi}_b^{(A)} & \boldsymbol{\Phi}_b^{(B)} \end{bmatrix} = \mathbf{U} \mathbf{S} \mathbf{V}^T. \quad (18)$$

Note, that an appropriate selection of the truncation limit is required in Eq. (18) for both modal bases, to ensure that a relevant dynamic behaviour is contained, considering the frequency band of interest.

SVD provides the most efficient way to capture the dominant components of an infinite-dimensional processes with a finite and often relatively small number of contributions [19, 20]. Therefore, it is reasonable to expect that the input matrix  $\mathbf{P}$  can be well approximated by  $N_c \ll N^{(A)} + N^{(B)}$  singular contributions:

$$\mathbf{P} \approx \tilde{\mathbf{P}}_{N_c} = \mathbf{U}_{N_c} \mathbf{S}_{N_c} \mathbf{V}_{N_c}^T. \quad (19)$$

Since the mode shapes are considered in the SVD input matrix, the quality of the approximation can be evaluated using the established modal assurance

---

<sup>7</sup>Within the paper, only real modes are considered, therefore conjugate transpose  $[\ ]^H$  is replaced by transpose  $[\ ]^T$  when considering SVD in Eqs. (18) and (19).

criterion (MAC) [21]. For the given  $N_c$ , the MAC values for all the mode shapes of substructures A and B can be evaluated:

$$\mathbf{d}_{N_c} = \text{MAC} \left( \mathbf{P}, \tilde{\mathbf{P}}_{N_c} \right) \quad (20)$$

In the proposed weak formulation of **singular vector constraints (SVCs)**, the physical motion at the interface is projected onto the  $N_c$  dominant left singular vectors. These vectors are obtained by the SVD of the combined modal bases of the substructures A and B<sup>8</sup>. Unlike with the modal-constraint approach, where the weakening matrix is based on the global motion of a single substructure, the set of the first  $N_c$  left singular vectors embodies the most dominant interface motion of both substructures. The unnecessary/redundant information is omitted. Therefore, these singular vectors are expected to form a consistent projection basis for the constraint-weakening process:

$$\mathbf{W}_{\mathbf{U}}^{(A,B)} = \mathbf{U}_{N_c}^{(A,B)T}. \quad (21)$$

A weak singular vector formulation of the compatibility condition (15) can be written as follows:

$$\mathbf{U}_{N_c}^T \mathbf{u}_b^{(A)} = \mathbf{U}_{N_c}^T \mathbf{u}_b^{(B)}. \quad (22)$$

Left singular vectors, that capture the dominant interface dynamics, typically prove to form a consistent basis for the constraint-weakening process. However, a proper estimate of the number of dominant singular vectors is of great importance. Based on the presented analyses, it transpires that the best quality of substructuring prediction is typically obtained if the cut-off limit is selected in the range where the magnitude of the singular values is reduced by 80–90%. In the following, this empirical criterion is used to determine the number of considered left singular vectors in the weakening matrix. The proposed methodology is schematically depicted in Figure 2.

---

<sup>8</sup>Since the matrix  $\mathbf{U}_{N_c}$  is real and orthonormal, the calculation of the generalized inverse can be simplified to transposition. As a result, a single singular vector defines a single constraint equation.

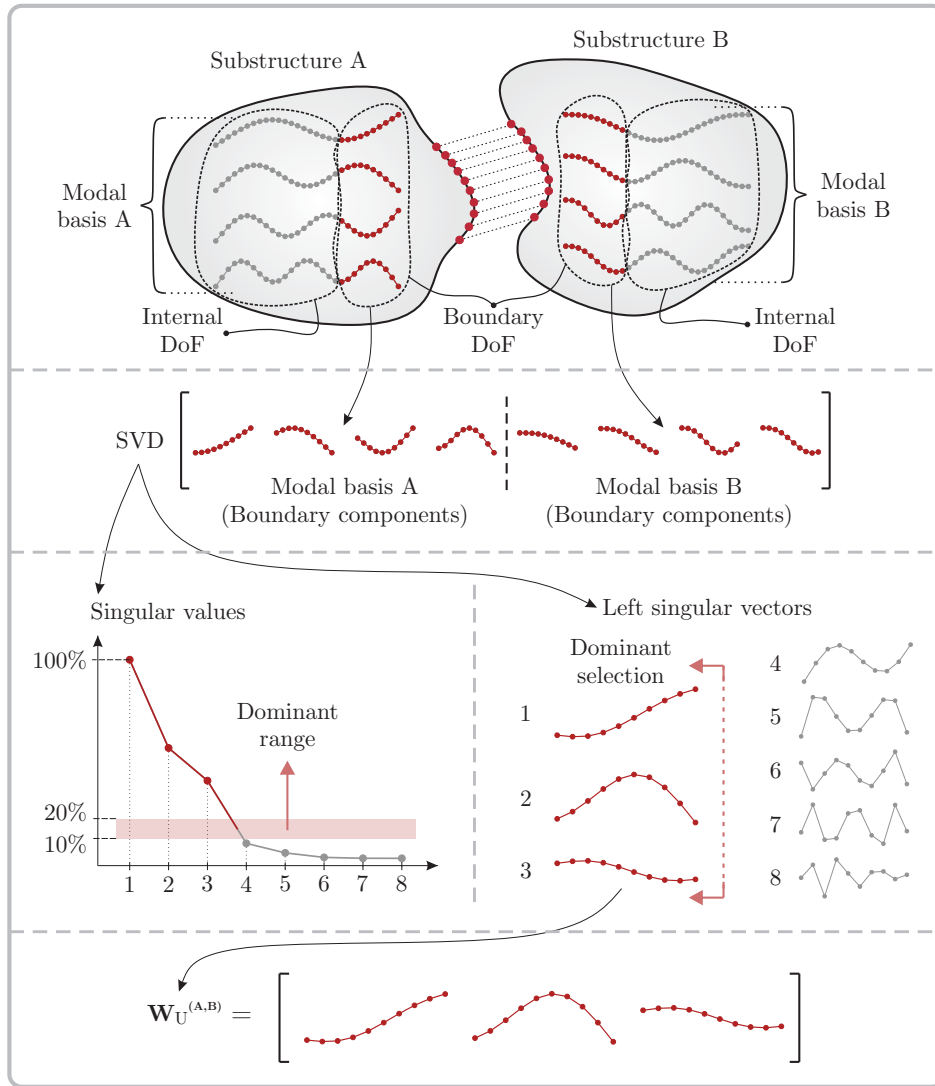


Figure 2: Schematic depiction of the proposed SVC approach.

### 3.2. Direct Coupling

In this section the general equations of modal substructuring are applied to the direct coupling of substructures A and B (Figure 1). Within the paper, the substructuring prediction of the damping properties is not discussed; therefore, the damping-related terms are omitted in the following.

The equation of motion Eq. (6) can be written as<sup>9</sup>:

$$\begin{bmatrix} \mathbf{I}^{(A)} & \mathbf{0} \\ \mathbf{0} & \mathbf{I}^{(B)} \end{bmatrix} \begin{bmatrix} \ddot{\boldsymbol{\eta}}^{(A)} \\ \ddot{\boldsymbol{\eta}}^{(B)} \end{bmatrix} + \begin{bmatrix} \boldsymbol{\omega}_r^{2(A)} & \mathbf{0} \\ \mathbf{0} & \boldsymbol{\omega}_r^{2(B)} \end{bmatrix} \begin{bmatrix} \boldsymbol{\eta}^{(A)} \\ \boldsymbol{\eta}^{(B)} \end{bmatrix} = \begin{bmatrix} \mathbf{f}_m^{(A)} \\ \mathbf{f}_m^{(B)} \end{bmatrix} + \begin{bmatrix} \mathbf{g}_m^{(A)} \\ \mathbf{g}_m^{(B)} \end{bmatrix}, \quad (23)$$

where,  $\mathbf{I}^{(s)}$  is an identity (mass) matrix and  $\boldsymbol{\omega}_r^{2(s)}$  is a diagonal matrix of the substructure's eigenvalues.

Considering Eq. (11) and assuming the collocation of the boundary DoF on substructures A and B, a weak compatibility condition can be written as:

$$\mathbf{W} \begin{bmatrix} [\mathbf{I}_b, \mathbf{0}_i]^{(A)} & [-\mathbf{I}_b, \mathbf{0}_i]^{(B)} \end{bmatrix} \begin{bmatrix} \boldsymbol{\Phi}^{(A)} & \mathbf{0} \\ \mathbf{0} & \boldsymbol{\Phi}^{(B)} \end{bmatrix} \begin{bmatrix} \boldsymbol{\eta}^{(A)} \\ \boldsymbol{\eta}^{(B)} \end{bmatrix} = \mathbf{0}. \quad (24)$$

Within the direct-coupling examples in Section 4, three different formulations of weakening matrices are considered, following Eqs. (16) and (21):

- Case 1: Weak modal constraints, considering the first  $N_c$  mode shapes of substructure A:  $\mathbf{W} = \mathbf{W}_{\boldsymbol{\Phi}}^{(A)} = \boldsymbol{\Phi}_{b, N_c}^{(A)\dagger}$
- Case 2: Weak modal constraints, considering the first  $N_c$  mode shapes of substructure B:  $\mathbf{W} = \mathbf{W}_{\boldsymbol{\Phi}}^{(B)} = \boldsymbol{\Phi}_{b, N_c}^{(B)\dagger}$
- Case 3: Weak singular constraints, considering the first  $N_c$  left singular vectors, obtained by the SVD on the concatenated mode shapes of substructures A and B:  $\mathbf{W} = \mathbf{U}_{N_c}^{(A,B)T}$

### 3.3. Transmission Simulator Method

The transmission simulator method was developed to combine experimentally derived modal models with analytical (numerical) ones [5, 13]. A flexible fixture or transmission simulator (TS) is introduced to the substructuring procedure. TS is attached to the experimental substructure B to improve its modal

---

<sup>9</sup>Note that for a substructure  $s$ , a (truncated) set of  $N^{(s)}$  mass-normalized free-interface mode shapes  $\boldsymbol{\Phi}^{(s)}$  is considered as a reduction matrix.

basis. The combined B+TS substructure is denoted as BTS. TS can also be attached to the numerical substructure A (thereby forming the ATS structure), in a way to occupy the same space as on the experimental substructure<sup>10</sup>. Since a numerical model of TS is also available, the coupled response of the AB structure is obtained by one coupling and two decoupling steps between the substructures ATS, BTS and TS, as depicted in Figure 3.

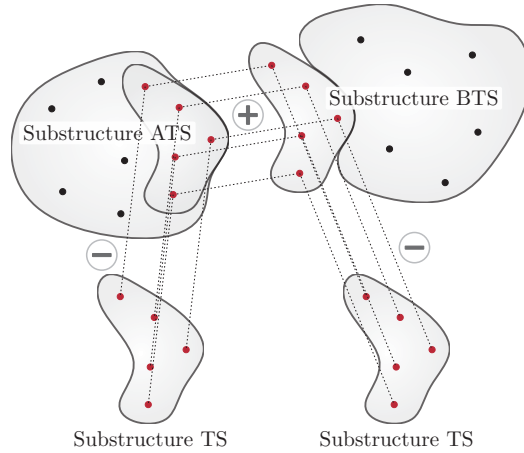


Figure 3: Depiction of coupling/decoupling procedure in the transmission simulator method.

In order to improve the substructuring prediction using the transmission simulator, the physical design should comply with the following guidelines [13, 22]:

- The interface geometry and material of the TS should be compliant to the real coupled interface properties, in order to capture the stiffness and damping of the joint.
- The TS should be as simple as possible to model and fabricate.
- The TS should stress the joint in the manner that roughly resembles the dynamics of the real coupled structure.

<sup>10</sup>Physically, such a coupling is not possible; however, it is easily applicable at the level of numerical modelling. The coupling of A and TS (and afterwards also decoupling) is not necessarily required; however such a case will be discussed in the following.

System of equations of motion for the given coupling/decoupling procedure, considering Eq. (6), is given as:

$$\begin{aligned}
& \begin{bmatrix} \mathbf{I}^{(\text{ATS})} & \mathbf{0} & \mathbf{0} & \mathbf{0} \\ \mathbf{0} & -\mathbf{I}^{(\text{TS})} & \mathbf{0} & \mathbf{0} \\ \mathbf{0} & \mathbf{0} & \mathbf{I}^{(\text{BTS})} & \mathbf{0} \\ \mathbf{0} & \mathbf{0} & \mathbf{0} & -\mathbf{I}^{(\text{TS})} \end{bmatrix} \begin{bmatrix} \ddot{\boldsymbol{\eta}}^{(\text{ATS})} \\ \ddot{\boldsymbol{\eta}}^{(\text{TS})} \\ \ddot{\boldsymbol{\eta}}^{(\text{BTS})} \\ \ddot{\boldsymbol{\eta}}^{(\text{TS})} \end{bmatrix} + \\
& \begin{bmatrix} \boldsymbol{\omega}_r^{2(\text{ATS})} & \mathbf{0} & \mathbf{0} & \mathbf{0} \\ \mathbf{0} & -\boldsymbol{\omega}_r^{2(\text{TS})} & \mathbf{0} & \mathbf{0} \\ \mathbf{0} & \mathbf{0} & \boldsymbol{\omega}_r^{2(\text{BTS})} & \mathbf{0} \\ \mathbf{0} & \mathbf{0} & \mathbf{0} & -\boldsymbol{\omega}_r^{2(\text{TS})} \end{bmatrix} \begin{bmatrix} \boldsymbol{\eta}^{(\text{ATS})} \\ \boldsymbol{\eta}^{(\text{TS})} \\ \boldsymbol{\eta}^{(\text{BTS})} \\ \boldsymbol{\eta}^{(\text{TS})} \end{bmatrix} = \begin{bmatrix} \mathbf{f}_m^{(\text{ATS})} \\ \mathbf{f}_m^{(\text{TS})} \\ \mathbf{f}_m^{(\text{BTS})} \\ \mathbf{f}_m^{(\text{TS})} \end{bmatrix} + \begin{bmatrix} \mathbf{g}_m^{(\text{ATS})} \\ \mathbf{g}_m^{(\text{TS})} \\ \mathbf{g}_m^{(\text{BTS})} \\ \mathbf{g}_m^{(\text{TS})} \end{bmatrix}, \tag{25}
\end{aligned}$$

where for a substructure ( $s$ ),  $\mathbf{I}^{(s)}$  is an identity matrix and  $\boldsymbol{\omega}_r^{2(s)}$  is a diagonal matrix of the substructure's eigenvalues. Considering Eq. (11) and assuming the collocation of the boundary DoF of substructures ATS, BTS and TS, a weak compatibility condition can be written as:

$$\begin{aligned}
& \begin{bmatrix} \mathbf{W}_1 & \mathbf{0} & \mathbf{0} \\ \mathbf{0} & \mathbf{W}_2 & \mathbf{0} \\ \mathbf{0} & \mathbf{0} & \mathbf{W}_3 \end{bmatrix} \begin{bmatrix} [\mathbf{I}_b, \mathbf{0}_i]^{(\text{ATS})} & [-\mathbf{I}_b, \mathbf{0}_i]^{(\text{TS})} & \mathbf{0}^{(\text{BTS})} & \mathbf{0}^{(\text{TS})} \\ \mathbf{0}^{(\text{ATS})} & \mathbf{0}^{(\text{TS})} & [\mathbf{I}_b, \mathbf{0}_i]^{(\text{BTS})} & [-\mathbf{I}_b, \mathbf{0}_i]^{(\text{TS})} \\ [\mathbf{I}_b, \mathbf{0}_i]^{(\text{ATS})} & \mathbf{0}^{(\text{TS})} & [-\mathbf{I}_b, \mathbf{0}_i]^{(\text{BTS})} & \mathbf{0}^{(\text{TS})} \end{bmatrix} \\
& \begin{bmatrix} \boldsymbol{\Phi}^{(\text{ATS})} & \mathbf{0} & \mathbf{0} & \mathbf{0} \\ \mathbf{0} & \boldsymbol{\Phi}^{(\text{TS})} & \mathbf{0} & \mathbf{0} \\ \mathbf{0} & \mathbf{0} & \boldsymbol{\Phi}^{(\text{BTS})} & \mathbf{0} \\ \mathbf{0} & \mathbf{0} & \mathbf{0} & \boldsymbol{\Phi}^{(\text{TS})} \end{bmatrix} \begin{bmatrix} \boldsymbol{\eta}^{(\text{ATS})} \\ \boldsymbol{\eta}^{(\text{TS})} \\ \boldsymbol{\eta}^{(\text{BTS})} \\ \boldsymbol{\eta}^{(\text{TS})} \end{bmatrix} = \mathbf{0}. \tag{26}
\end{aligned}$$

Within the experimental-analytical study in Section 5, two different formulations of weakening matrices are considered:

- Case 1: Following the MCFS approach in [5], the modal basis of the substructure TS is used to construct the weakening matrix:

$$\mathbf{W}_1 = \mathbf{W}_2 = \mathbf{W}_3 = \boldsymbol{\Phi}_b^{(\text{TS})\dagger}$$

- Case 2: Within the proposed SVC approach, the weakening matrix for a certain coupling/decoupling step is constructed from the dominant left singular vectors. The  $N_c$  value for each step is selected according to the proposed MAC-based criterion:

$$\begin{aligned}\mathbf{W}_1 &= \mathbf{U}_{N_{c_1}}^{(ATS,TS)T} \\ \mathbf{W}_2 &= \mathbf{U}_{N_{c_2}}^{(BTS,TS)T} \\ \mathbf{W}_3 &= \mathbf{U}_{N_{c_3}}^{(ATS,BTS)T}\end{aligned}$$

#### 4. Numerical examples

In this section the direct coupling of substructures A and B is presented in three examples. The results using the proposed SVCs are compared to the established modal constraint approach. Substructure A is considered as the numerical substructure with an arbitrary number of available modes, whereas for the experimental (here simulated) substructure B, the upper frequency limit is set to 8 kHz. In the reduction basis, all the mass-normalized free-interface mode shapes up to the selected frequency limit are considered. All the substructures are modelled with solid finite elements (3 displacement DoFs/node). The reference (AB) structure model consists of two substructures, perfectly bonded at the interface with approx. 2500 nodes, simulating a homogeneous joint. The substructuring procedure is performed considering multiple connection points' displacements and applying weak constraint formulation. With such an approach, the need for explicit consideration of rotational degrees of freedom at the interface is avoided [5].

A mode-by-mode comparison of the reference modal parameters and the substructuring prediction can be difficult due to the possibility of mode-order changes and/or the occurrence of spurious modes. Therefore, the coherence function [23] is used instead to compare the substructuring prediction ( $Y_{\text{sub}}$ ) with the reference ( $Y_{\text{ref}}$ ) frequency-response function ( $[\ ]^*$  denotes the complex conjugate's value):

$$\text{COH}(Y_{\text{ref}}, Y_{\text{sub}}) = \frac{(Y_{\text{ref}} + Y_{\text{sub}})(Y_{\text{ref}}^* + Y_{\text{sub}}^*)}{2(Y_{\text{ref}} Y_{\text{ref}}^* + Y_{\text{sub}} Y_{\text{sub}}^*)}, \quad (27)$$

Three types of substructures are considered, i.e., two variations of the numerical substructure (A1 and A2) and an experimental substructure (B). The corresponding geometrical models are depicted in Figure 4. On the numerical substructures A1 and A2, 48 and 63 connecting points (3 DoF) were selected, respectively. For either case, the corresponding number of coincidental points is considered on the experimental substructure B. The selected coupled upper frequency limit is set to 4 kHz.

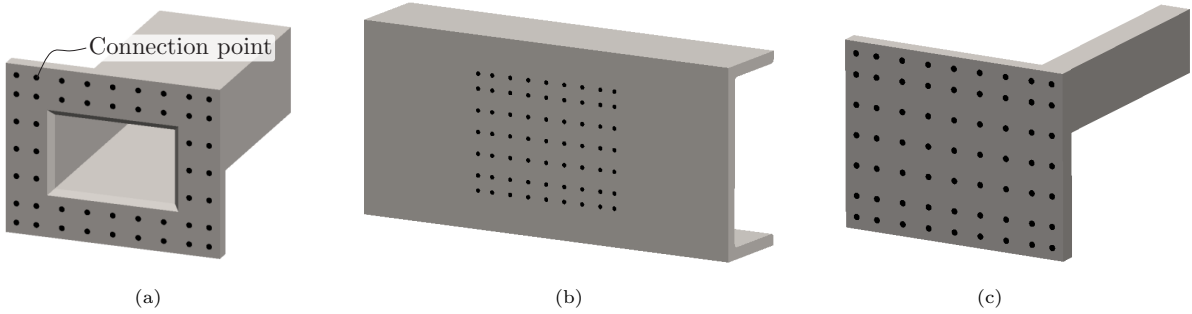


Figure 4: CAD models: (a) Substructure A1; (b) Substructure A2; (c) Substructure B.

The applicability of the proposed methodology is tested with respect to the considered numerical truncation limit and the change of the numerical substructures' geometry, boundary conditions and the number of connecting points.

#### 4.1. Numerical example 1

In the first example, the direct coupling of substructures A1 and substructure B is analysed, as depicted in Figure 5a. For both substructures, the same 8-kHz upper frequency limit is considered, resulting in 30 and 17 mass-normalized mode shapes in the reduction basis for the substructures A1 and B, respectively. Assuming three displacement DoFs per node, 144 physical constraints can be applied for 48 connecting points. Singular values, obtained by SVD of the concatenated modal bases of substructures A1 and B, are depicted in Figure 5b. The grey shaded area indicates the proposed cut-off range, where the singular value magnitude decreases to 20–10%, relative to the first component. User selection is required in this area, for which a mid-range selection is typically

applied <sup>11</sup>, denoted by a red dashed line.

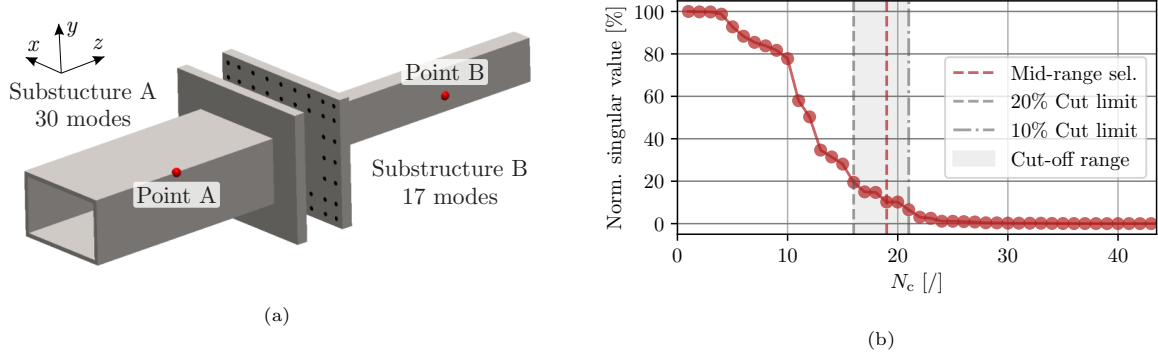


Figure 5: Example 1 - (a) Substructures A and B; (b) Normalized singular values.

To demonstrate the efficiency of the SVD, the approximation (Eq. ( 19)) of the SVD input matrix is obtained using the selected  $N_c = 19$  dominant singular contributions. Using Eq. (20), the accuracy of the approximation is verified, as depicted in Figure 6. With the exception of three individual mode shapes, which can presumably be considered less significant with respect to the interface motion, most MAC values are very close to 1.

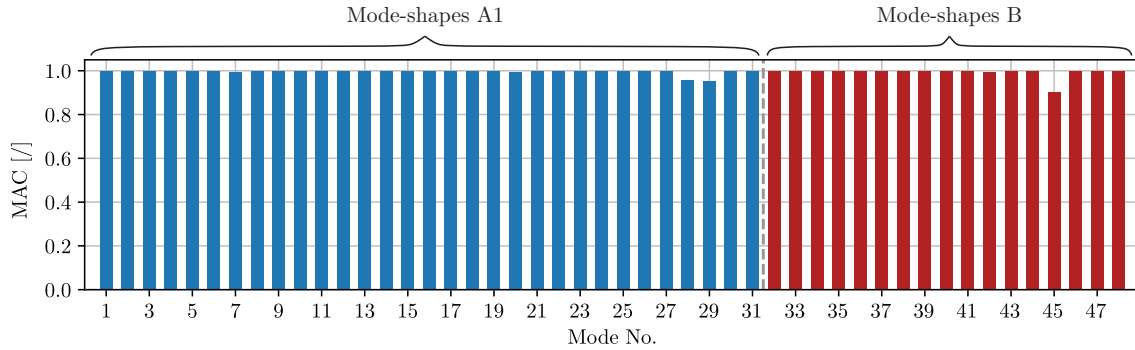


Figure 6: MAC comparison of SVD input and approximation, obtained by  $N_c = 19$  dominant singular contributions.

<sup>11</sup>The proposed mid-range selection does not necessarily provide an optimal selection. Better results may be achieved by manually selecting the cut-off limit, considering the corresponding singular value curve.

For each of the points A and B (locations are depicted in Figure 5), six distinct FRFs can be obtained<sup>12</sup>. The accuracy of the coupling prediction is indicated by the average coherence (Eq. (27)) of all six FRFs, obtained at the individual point. The aim is to identify the effect of the number of applied weak constraints, considering the three different approaches:

- (a) MC-A: modal constraints, using the first  $N_c$  mode shapes of substr. A1,
- (b) MC-B: modal constraints, using the first  $N_c$  mode shapes of substr. B,
- (c) SVC: singular vector constraints, using the first  $N_c$  left singular vectors, obtained by the proposed approach in Section 3.1.

The results are given in Figure 7. Note, that the proposed cut-off range only applies to the proposed SVC approach, while in the MC approach a full modal basis (e.g.,  $N_c = 30$  or  $N_c = 17$  for modal bases A and B, respectively) is typically considered. A comparison of the different weakening approaches indicates that both the selection of the weakening basis and its dimension can significantly affect the quality of the substructuring prediction.

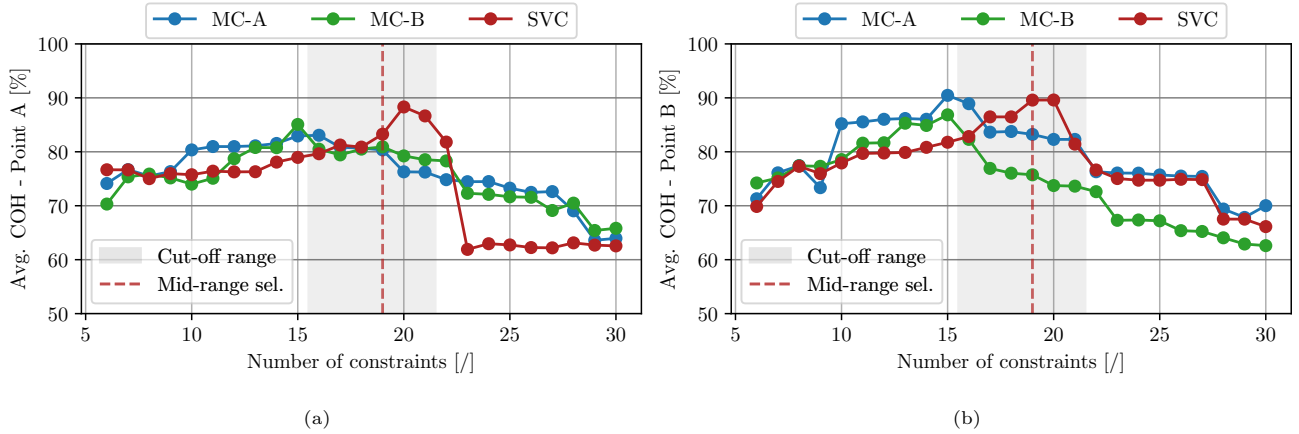


Figure 7: Example 1 - Average coherence (based on the six distinct FRFs at a point of interest)  
(a) Point A; (b) Point B.

<sup>12</sup>When synthesizing FRFs for a single node with  $x, y, z$  displacement DoFs and assuming reciprocity, six distinct input-output combinations ( $xx, yy, zz, xy, xz$  and  $yz$ ) are possible.

By comparing the MC-A and MC-B approaches, generally, the results are quite similar, which is to be expected, since the substructures A1 and B are geometrically relatively similar and thus form comparable weakening bases. However, especially at point B (Fig. 7b), slightly higher coherence values can be achieved by using the modal basis of substructure A. This can probably be attributed to its richer modal basis. In both cases it is evident that the optimal coherence values are achieved in the range of  $N_c = 15$ . Compared to the results obtained by the full 17- or 30-mode basis for substructures A and B, respectively, significantly lower coherence values are achieved. This is especially evident in Figure 7b, where the difference between the optimal and full-basis MC-A result is close to 20%.

The SVC results demonstrate that the highest coherence values for both points, A and B, are located within the proposed cut-off range. Despite the fact that the range of optimal values is relatively narrow, a mid-range selection within the proposed criterion range provides a coherence value that is comparable to the optimal values of the MC approach. Furthermore, the comparison of the MC and SVC results indicates that when an optimal number of singular vector constraints is applied, comparable or slightly higher coherence values can be achieved, compared to the optimal modal constraint results.

For the user-selected  $N_c = 19$  using the SVC approach, the coupled predictions of the  $y$  direction driving point FRFs at points A and B are given in Figure 8. The match with the reference is relatively good at 81% and 91% mean coherence value for the points A and B, respectively.

In a real-life scenario, the user has no insight into the above analysis to estimate the optimal number of applied constraints within the MC approach. Hereby, using the full modal basis (or by random truncation selection) within the established MC approach, the accuracy of the substructuring prediction can be significantly lower, compared to the proposed SVC approach.

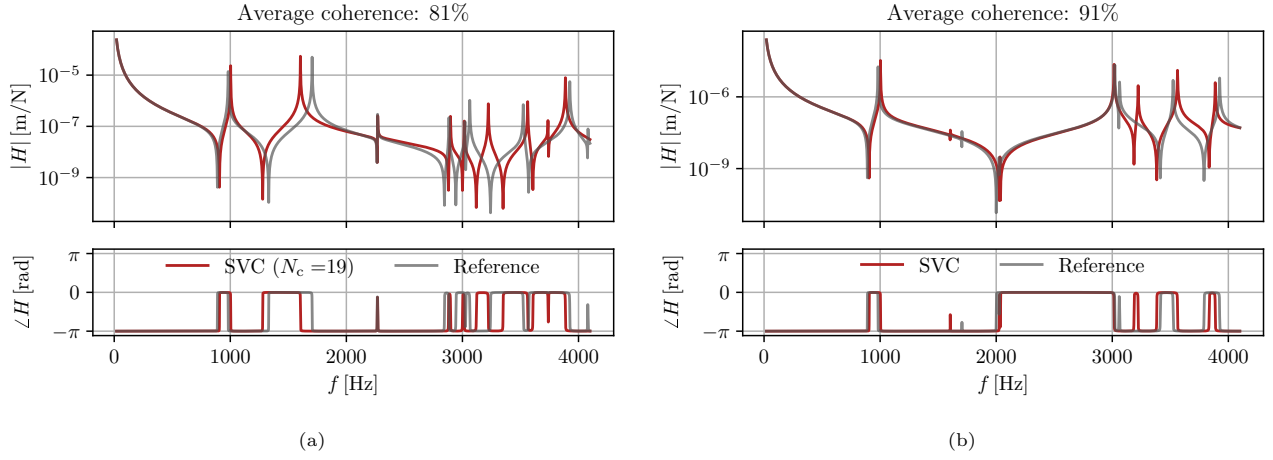


Figure 8: Example 1 - Driving point FRF for the  $y$  direction, using SVC approach ( $N_c = 19$ ): (a) Point A; (b) Point B.

#### 4.2. Numerical example 2

In the second example a similar coupling procedure is performed to that in Example 1. The applicability of the proposed method is tested with respect to the changing truncation limit of the numerical substructure A1. For example, we can simply consider doubling the number of modes in the modal basis of substructure A1 and retain the 8-kHz upper frequency limit for the experimental substructure B (Figure 9a). In Figure 9b, the corresponding singular values are depicted together with the shaded area, indicating the proposed cut-off range. The user-selected value of  $N_c = 23$  is indicated by a red dashed line. For all three considered constraint-weakening approaches, the average coherence values for the FRFs at points A and B are given in Figure 10. Comparing the MC-A and MC-B, generally some slight advantage can be attributed to the modal basis of the substructure A1. No significant differences can be observed when comparing the optimal MC and SVC coherence values. However, within the MC approach, there is no guarantee to select an appropriate truncation limit to achieve the optimal results. The results of both the MC-A and MC-B approaches indicate that inappropriate selection can lead to a significant reduction in accuracy. On the other hand, by applying the proposed cut-off limit

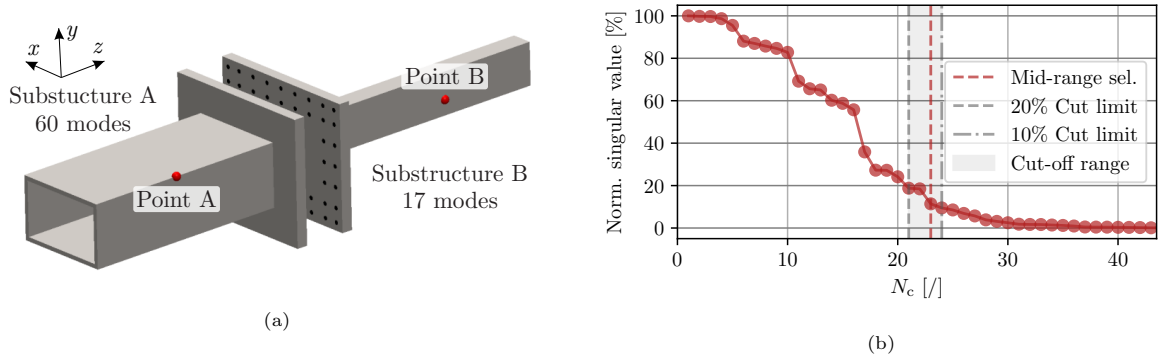


Figure 9: Example 2 - (a) Substructures A and B; (b) Normalized singular values.

within the SVC approach, close-to-optimal results are obtained.

Compared to the results presented in Example 1 (Fig. 7), the maximum SVC coherence values reach approximately the same value (about 90%).

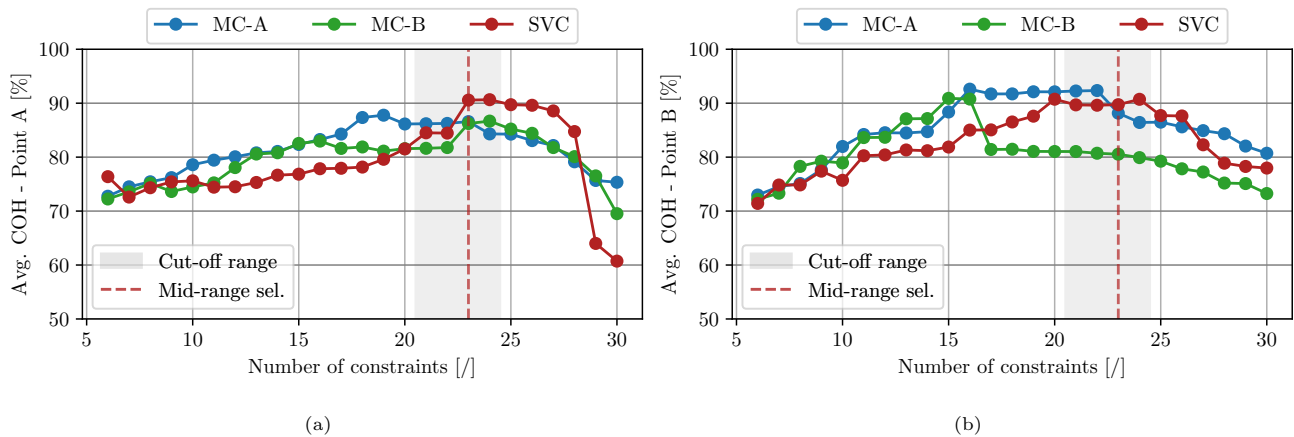


Figure 10: Example 2 - Average coherence (based on the six distinct FRFs at a point of interest) (a) Point A; (b) Point B.

When considering analytical substructures, typically the truncation limit can be arbitrarily selected. In order to be able to draw some clear conclusions about the effects of changing the truncation criterion, the analysis is performed with respect to the highest average coherence values (Figure 11a) and the corresponding optimal number of the applied singular vector constraints (Figure 11b).

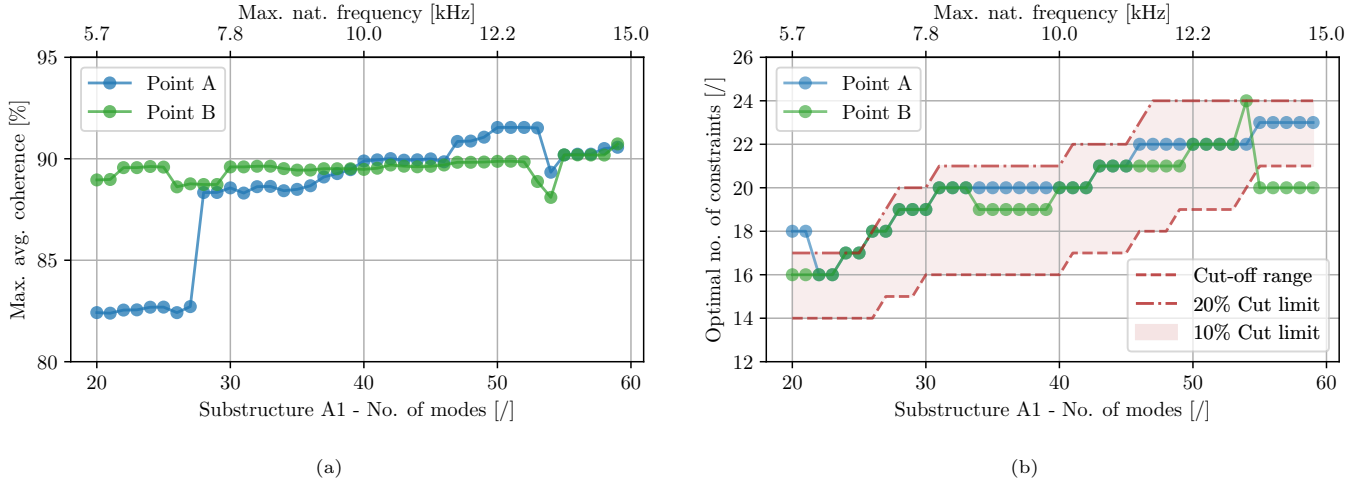


Figure 11: SVC approach - Effect of the numerical substructure's truncation limit: (a) Highest average coherence values; (b) Optimal number of singular constraints.

Given the maximum average coherence values at point A (Figure 11a), the results indicate that a moderate increase (to roughly 1.5 times the experimental frequency range of interest) can prove beneficial. This mostly applies to the increased accuracy of the substructuring prediction in the DoF, located on the numerical substructure. However, no significant changes can be observed in the highest coherence values for point B. In Figure 11b, the red shaded area indicates the proposed cut-off range, where the singular value magnitude decreases to 20–10%. Given the locations of the optimal number of constraints in the analysed frequency range, we can conclude that the proposed criterion is suitable for estimating the number of required constraints. Note, that the introduction of significantly higher frequency (numerical) dynamics seems ineffective or not relevant to the substructuring process in the given frequency band. In some cases it can result in a significantly lower accuracy of the substructuring prediction. If for some reason a high-frequency range is considered in the reduction basis, the truncation near the frequency band of interest is required in Eq. (18).

### 4.3. Numerical example 3

In the third example, several changes are applied compared to the previous examples, to test the robustness of the proposed SVC approach. The geometry of the numerical substructure is replaced with the A2 model and a fixed support is applied, as depicted in Figure 12a. Considering the change in geometry, the number of connecting point is increased to 63. The 8-kHz upper frequency limit is retained for the experimental substructure B. Based on the conclusions from the previous example, a truncation limit of 12 kHz (40 modes) is applied to the numerical substructure.

In Figure 12b, the corresponding singular values are depicted together with the shaded area indicating the proposed cut-off range. The user-selected value of  $N_c = 19$  is denoted by a red dashed line.

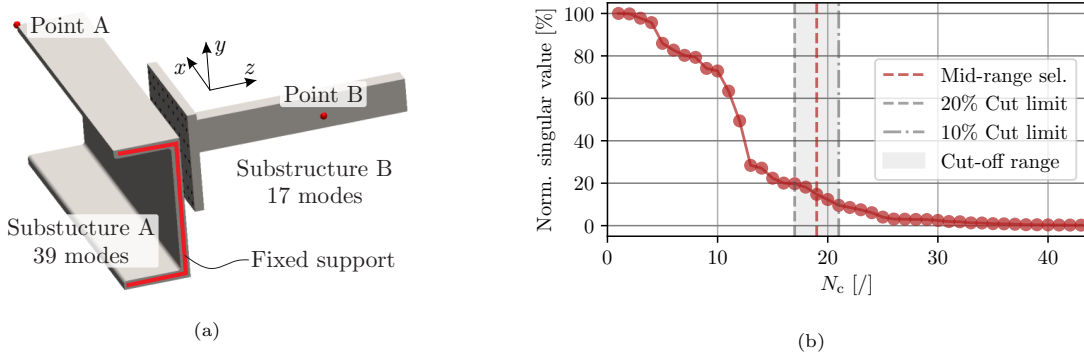


Figure 12: Example 3 - (a) Substructures A and B; (b) Truncation criterion.

For all three considered constraint-weakening approaches, the average coherence values for the FRFs at points A and B are given in Figure 13. The results show that for both points, the range of maximum coherence values coincides with the proposed shaded criterion range. This indicated that the proposed approach and cut-off criterion are also applicable in different substructuring cases.

In this case the comparison of the optimal results obtained using the three approaches indicates that the proposed SVC approach seems to provide higher accuracy for the substructuring prediction. For example, when considering the

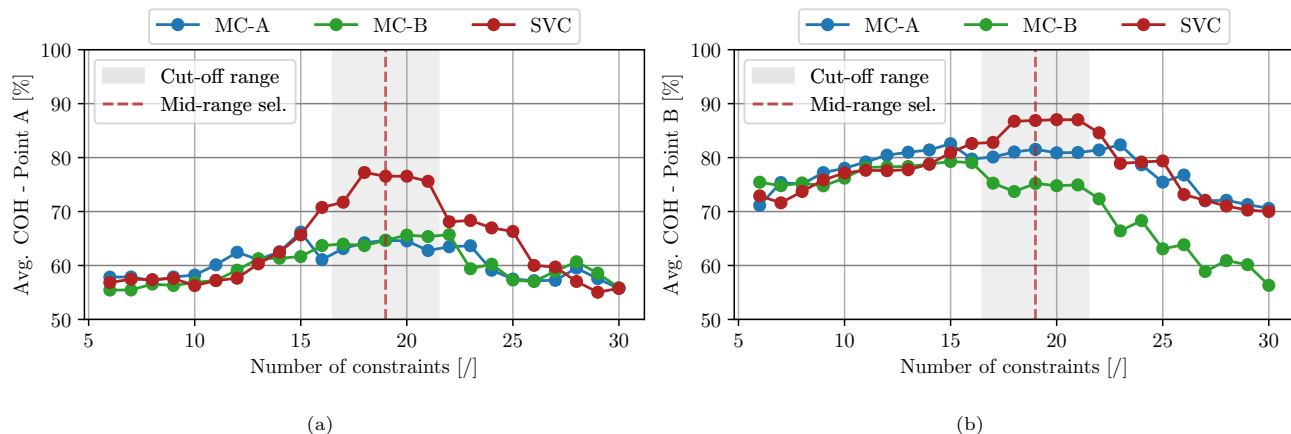


Figure 13: Example 3 - Average coherence (based on the six distinct FRFs at a point of interest) (a) Point A; (b) Point B.

average coherence values obtained using the full 17-mode basis of substructure B, the SVC approach provides over 10% higher accuracy at both points, A and B. The reason for the better performance of the SVC approach can probably be attributed to the fact that the interface dynamics of the considered substructures are quite different. Therefore, the individual bases of substructures A and B do not seem optimal for the substructuring process, whereas the results are improved when both bases are taken into account within the SVC approach.

## 5. Experimental-numerical study

In this section the transmission simulator method is applied to the coupling procedure for numerical substructure A1 and the experimental substructure B, as depicted in Figure 14. Following the design guidelines in [13, 22], the transmission simulator (TS) is designed as a T-shaped structure. Thus the TS simulates real interface properties, roughly resembles the dynamics of substructure A1 and is easy to fabricate and model. The coupled substructures A1+TS and B+TS are denoted ATS and BTS, respectively. The accelerometers used in the experiment are included in the numerical models to ensure the highest-possible accuracy.

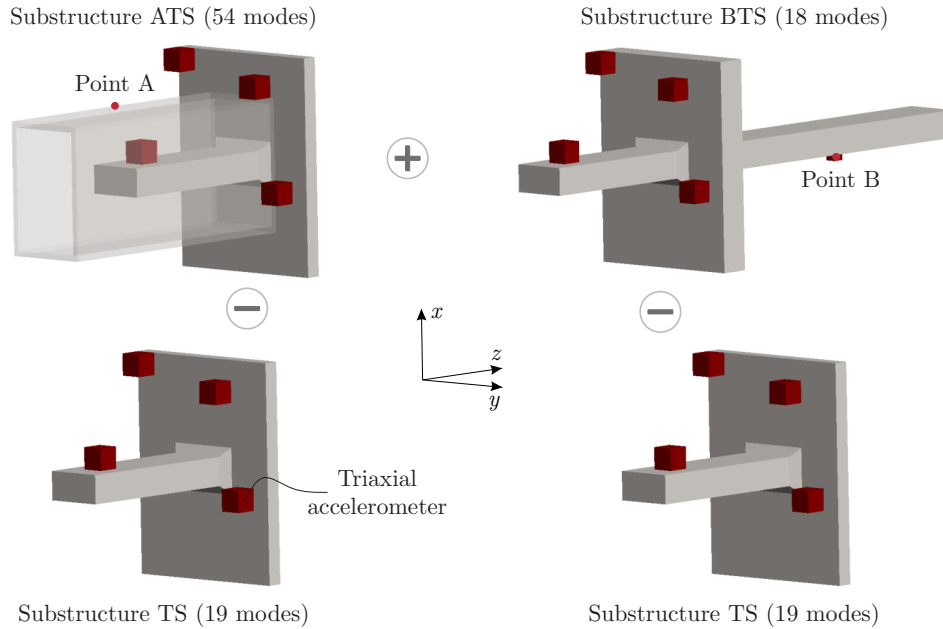


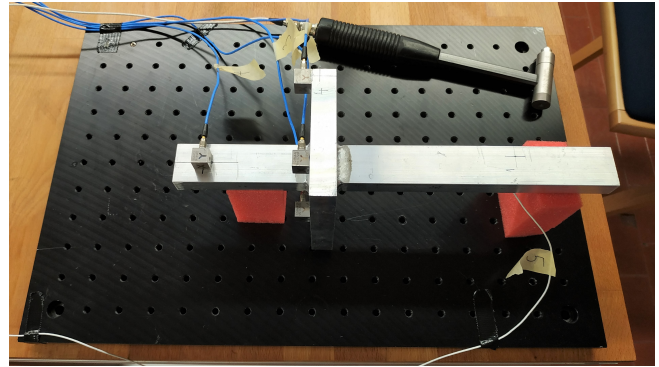
Figure 14: Transmission-simulator method - experiment depiction.

An actual BTS substructure was fabricated (Figure 15) and a multi-reference experimental modal analysis was performed [24] in the frequency range of 8 kHz. A PCB 086C03 impulse hammer was used for the impact excitation and four triaxial PCB 356A32 accelerometers, a triaxial Dytran 3133A1 accelerometer and a Polytec PDV-100 laser vibrometer were used to measure the structure's response. Approximately free-free boundary conditions were applied using the polyurethane-foam support blocks. Modal identification was performed using the Polymax algorithm [24].

In addition, an accurate numerical model of the BTS structure was built. Considering the frequency range of 8 kHz, 6 rigid-body and 13 flexible modes can be extracted. The comparison of the numerical and experimental models in terms of natural frequencies and MAC values for the first 13 flexible modes is given in Figure 16. The agreement in natural frequencies is very good for all the 13 modes, with the average absolute deviation below 1%. Similarly, the MAC values are close to 1 for the first 11 modes. For the higher modes, nonetheless,



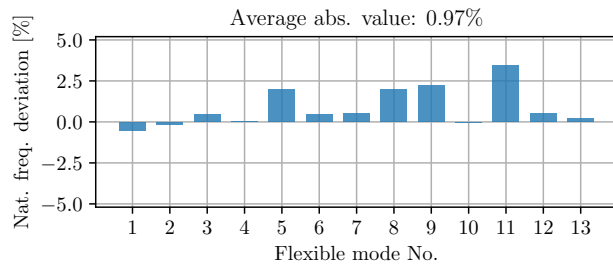
(a)



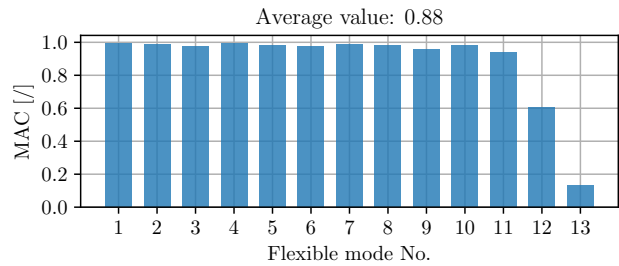
(b)

Figure 15: Experiment: (a) Setup; (b) BTS structure.

a significant drop can be observed. For the 12th mode, the MAC value of 0.61 is considered as acceptable; however, the 13th mode is excluded from further consideration due to the obvious inaccuracy of the identified mode shape.



(a)



(b)

Figure 16: Accuracy of the BTS structure numerical model compared to the experimental data: a) Natural frequency deviation; b) Modal assurance criterion (MAC).

Since the BTS structure is made of a homogeneous beam and plate, the B and TS substructure numerical models can be obtained by considering the material and geometrical properties of the validated numerical BTS substructure. A numerical coupled structure AB is considered as a reference, assuming a homogeneous joint. Based on the conclusions in Section 4, a truncation limit of 12 kHz is considered for the numerical substructures ATS and TS. The experimental

BTS model consists of the 6 rigid-body modes, obtained by the mass-properties of the structure, and the first 12 flexible experimental mass-normalized mode shapes (with the corresponding natural frequencies). The coupling procedure is performed at multiple discrete points, as depicted in Figure 17a. Using the available measuring equipment, the interface response at 4 points was measured using triaxial accelerometers (location shown as black dots), resulting in 12 measured displacement DoFs. The most prominent motion was expected in the out-of-plane direction, thus additional 25 out-of-plane measurements were performed using a laser vibrometer (locations shown as red dots) to capture this motion with higher spatial resolution. As a result, 37 physical constraints could be applied for each of the coupling/decoupling steps.

The aim of the study is to compare the substructuring prediction obtained using the established MCFS approach and the proposed SVC approach. In the first case, the (full) modal basis of substructure TS is used to obtain the weakening matrix. As an alternative, the applicability of the proposed singular vector constraints is explored. For each coupling/decoupling step, the first  $N_c$  dominant left singular vectors are used, obtained from the modal bases of the corresponding substructure pairs. The related singular value curves are given in Figures 17b–17d. The user-selected number of dominant singular vectors within the shaded range are denoted by the red dashed line.

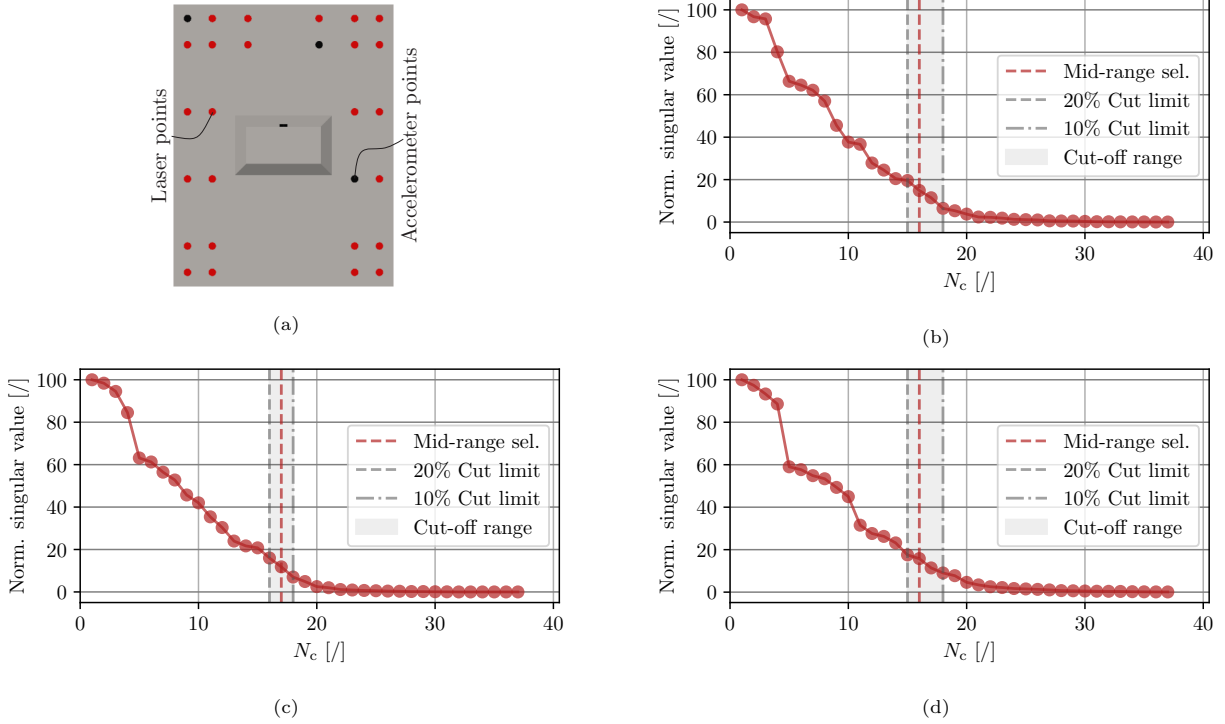


Figure 17: (a) Connecting points (laser - red, accelerometer - black); (b) Quality criterion - Step 1 (ATS-TS decoupling); (c) Quality criterion - Step 2 (BTS-TS decoupling); (d) Quality criterion - Step 3 (ATS-BTS coupling).

Applying the established MCFS, the coupled predictions of  $y$  direction driving point FRFs for points A and B are given in Figure 18 and compared to the reference. When the full modal basis (19 mode shapes) of the TS substructure is used to generate the weakening basis, an average coherence of 64% and 82% is obtained for points A and B, respectively, using the MCFS approach. For the proposed SVC approach, the coupled predictions of the  $y$  direction driving point FRFs for points A and B are given in Figure 19. Considering the user-selected  $N_{c_1} = 16$ ,  $N_{c_2} = 17$ ,  $N_{c_3} = 16$ , an average coherence of 85% and 87% is obtained for the points A and B, respectively.

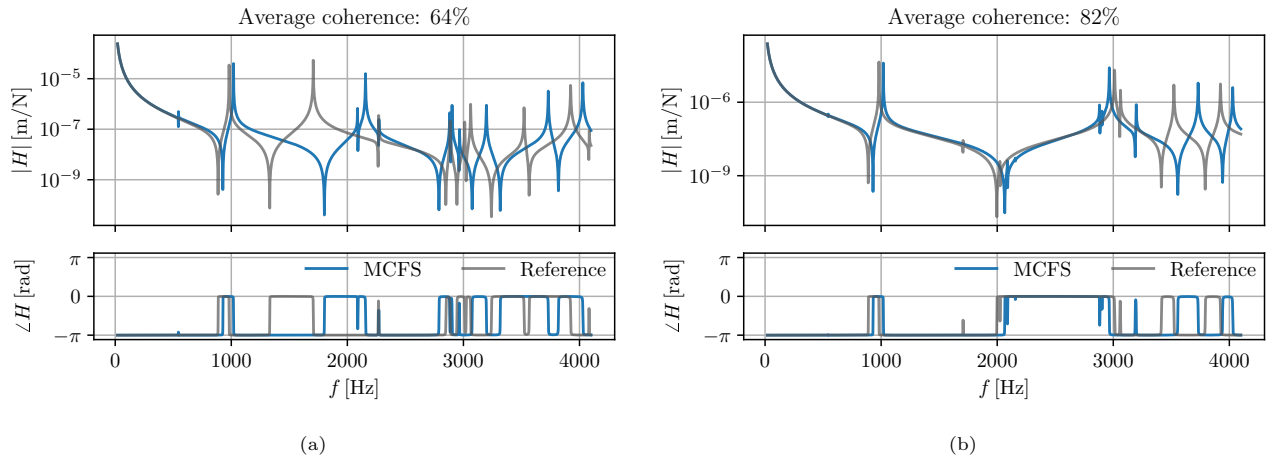


Figure 18: MCFS approach - Driving point FRF for the  $y$  direction: (a) Point A; (b) Point B.

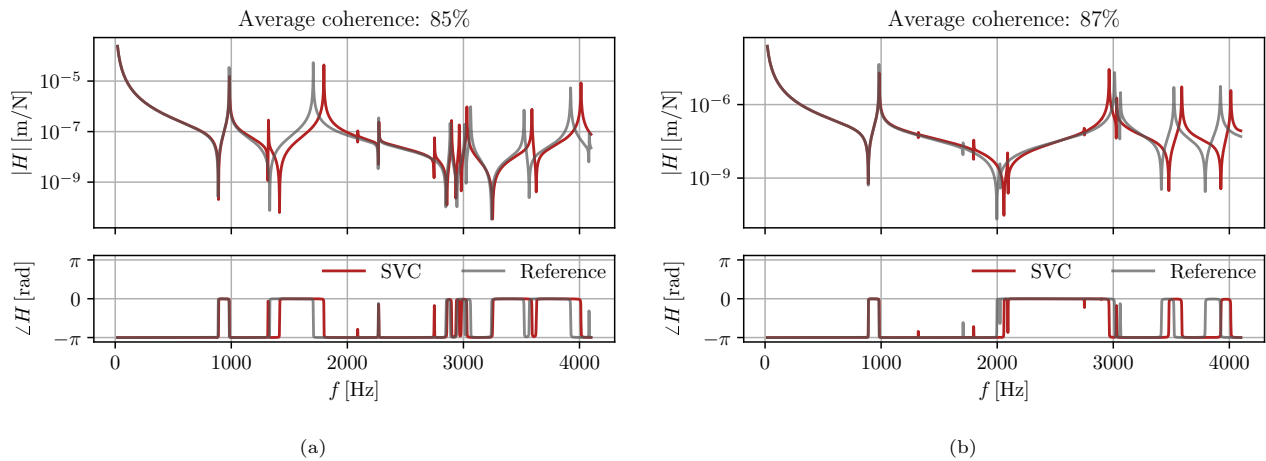


Figure 19: SVC approach - Driving point FRF for the  $y$  direction: (a) Point A; (b) Point B.

Within the presented MCFS results, the full modal basis of the TS substructure is considered for the weakening process. However, it turns out that the optimal MCFS-based results are obtained by using a reduced sub-basis of 12 modes. In such a case, the average coherence of 84% can be obtained for the given FRF at both points A and B, respectively. In this case the accuracy is very similar to the SVC results. In a real-life application, without prior knowledge

of the coupled dynamics, it is very demanding to estimate the optimal number of required modal constraints.

Within the MCFS [5], a general guideline proposes a truncation limit near the frequency band of interest. Therefore, an additional analysis is performed in which the truncation limit is varied in the  $\pm 2$  kHz range of the testable frequency limit of 8 kHz. At the lower (6 kHz) boundary of the range, 12 and 24 modes can be obtained for substructures TS and ATS, respectively. Similarly, 16 and 42 modes can be obtained for substructures TS and ATS at the upper (10-kHz) frequency limit. A comparison of the average coherence values for six distinct FRFs at point A, obtained by the MCFS and SVC approach for different truncation limit combinations, is given in Figure 20.

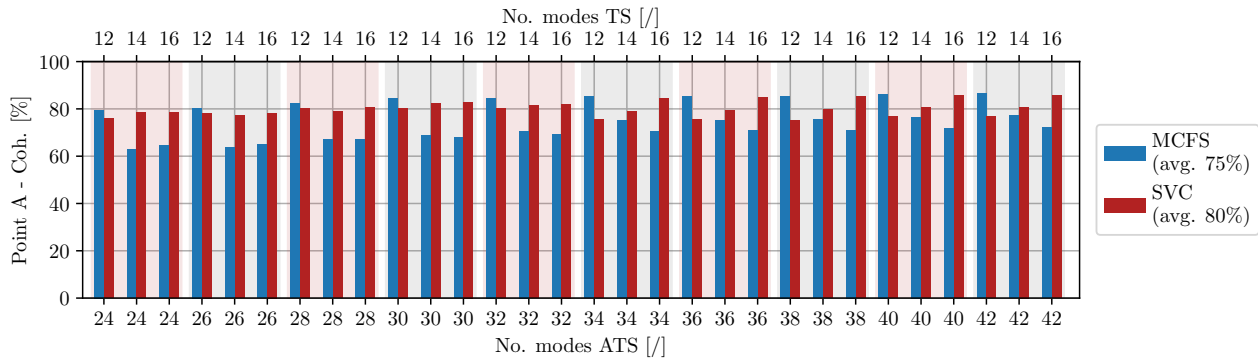


Figure 20: Consistency comparison of the MCFS and the proposed SVC approach.

Although the differences between the two approaches are not significant, the proposed SVC approach seems to provide greater consistency of results, when compared to the established MCFS. This is also evident from the comparison of the average achieved value for the different combinations of truncation limits, which is 75% for the MCFS approach and 80% for the SVC approach.

## 6. Conclusions

In this paper a new approach to the constraint-weakening process within modal substructuring is presented. It is based on singular value decomposition

and can also be seen as an extension of the established modal constraints (MCs) approach. Instead of a single modal basis being used in the weakening process, the proposed approach is based on the modal bases of two substructures that form a mutual interface. The concatenated interface-related components of the modal bases are submitted to SVD. The resulting dominant left singular vectors are selected, based on the proposed criterion, to form an orthonormal weakening basis. Thus, compared to the established MC approach, a potentially richer vector space is formed that captures the interface dynamics of both substructures and contains no redundant or insignificant contributions. Also, in the established MC approach, no general criterion is available to select the optimal modal sub-basis for the constraint-weakening process. However, in the proposed SVC approach, the number of dominant left singular vectors can be performed, based on the magnitude of the corresponding singular values.

The presented examples demonstrate the applicability of the proposed approach, when considering multi-point/continuous connections. The results indicate that with a proper application of singular vector constraints (SVCs), the equivalent of the higher accuracy of the substructuring prediction can be achieved even when compared to difficult-to-predict optimal MCs results. When considering a random selection of the truncation limit near the measurable frequency band, the application of SVC seems to ensure greater consistency of the results, compared to the MC. The proposed SVC approach, together with a suitable cut-off criterion, therefore proves to be beneficial when considering multi-point or continuous contact within the modal substructuring.

### **Acknowledgements**

The authors acknowledge partial financial support from the core research funding P2-0263 and the applied research project L2-1837, both financed by ARRS, the Slovenian research agency.

## References

- [1] P. Tiso, M. S. Allen, D. Rixen, T. Abrahamsson, M. Van der Seijs, R. L. Mayes, *Substructuring in Engineering Dynamics - Emerging Numerical and Experimental Techniques*, Springer, 2020.
- [2] D. Klerk, D. Rixen, S. Voormeeren, General framework for dynamic substructuring: History, review, and classification of techniques, *AIAA Journal* 46 (2008) 1169–1181.
- [3] D. Nicgorski, P. Avitabile, Experimental issues related to frequency response function measurements for frequency-based substructuring, *Mechanical Systems and Signal Processing* 24 (5) (2010) 1324–1337.
- [4] F. Trainotti, M. Haeussler, D. Rixen, A practical handling of measurement uncertainties in frequency based substructuring, *Mechanical Systems and Signal Processing* 144 (2020) 106846.
- [5] M. S. Allen, R. L. Mayes, E. J. Bergman, Experimental modal substructuring to couple and uncouple substructures with flexible fixtures and multi-point connections, *Journal of Sound and Vibration* 329 (23) (2010) 4891–4906.
- [6] Y. Chen, P. Avitabile, J. Dodson, Data consistency assessment function (dcaf), *Mechanical Systems and Signal Processing* 141 (2020) 106688.
- [7] M. Kodrič, G. Čepon, M. Boltežar, Experimental framework for identifying inconsistent measurements in frequency-based substructuring, *Mechanical Systems and Signal Processing* 154 (2021) 107562.
- [8] Z. Saeed, C. M. Firrone, T. M. Berruti, Joint identification through hybrid models improved by correlations, *Journal of Sound and Vibration* 494 (2021) 115889.
- [9] B. Starc, G. Čepon, M. Boltežar, The influence of washing machine-leg hardness on its dynamics response within component-mode synthesis techniques, *International Journal of Mechanical Sciences* 127 (2017) 23–30.

- [10] J. Cui, G. Zheng, An iterative state-space component modal synthesis approach for damped systems, *Mechanical Systems and Signal Processing* 142 (2020) 106558.
- [11] R. Mayes, E. Stasiunas, Lightly damped experimental substructures for combining with analytical substructures, in: *25th International Modal Analysis Conference (IMAC XXV)*, Orlando, Florida, 2007.
- [12] R. L. Mayes, M. Ross, P. S. Hunter, Examples of hybrid dynamic models combining experimental and finite element substructures, in: *28th International Modal Analysis Conference (IMAC XXVIII)*, Orlando, Florida, 2010.
- [13] R. L. Mayes, M. R. Ross, Advancements in hybrid dynamic models combining experimental and finite element substructures, *Mechanical systems and signal processing* 31 (2012) 56–66.
- [14] M. S. Allen, D. C. Kammer, R. L. Mayes, Metrics for diagnosing negative mass and stiffness when uncoupling experimental and analytical substructures, *Journal of Sound and Vibration* 331 (25) (2012) 5435–5448.
- [15] M. Pogačar, T. Bregar, G. Čepon, M. Boltežar, Weakening of the interface constraints in modal substructuring using singular value decomposition, in: *39th International Modal Analysis Conference (IMAC XXXIX)*, Online Conference, 2021.
- [16] J. Brunetti, W. D’Ambrogio, A. Fregolent, Dynamic coupling of substructures with sliding friction interfaces, *Mechanical Systems and Signal Processing* 141 (2020) 106731.
- [17] N. M. M. Maia, J. M. M. e Silva, *Theoretical and experimental modal analysis*, Research Studies Press, 1997.
- [18] P. Avitabile, *Modal testing: a practitioner’s guide*, John Wiley & Sons, 2017.

- [19] P. Holmes, J. L. Lumley, G. Berkooz, C. W. Rowley, *Turbulence, coherent structures, dynamical systems and symmetry*, Cambridge university press, 2012.
- [20] C. Wu, Y. Liang, W. Lin, H. Lee, S. Lim, A note on equivalence of proper orthogonal decomposition methods, *Journal of Sound and Vibration* 265 (5) (2003) 1103–1110.
- [21] R. J. Allemang, The modal assurance criterion—twenty years of use and abuse, *Sound and vibration* 37 (8) (2003) 14–23.
- [22] R. L. Mayes, M. Arviso, Design studies for the transmission simulator method of experimental dynamic substructuring, in: *International seminar on modal analysis*, 2010.
- [23] M. van der Seijs, D. van den Bosch, D. J. Rixen, D. de Klerk, An improved methodology for the virtual point transformation of measured frequency response functions in dynamic substructuring, *Proceedings of the 4th COMPDYN* (2014).
- [24] B. Peeters, H. Van der Auweraer, P. Guillaume, J. Leuridan, The polymax frequency-domain method: a new standard for modal parameter estimation?, *Shock and Vibration* 11 (3, 4) (2004) 395–409.